Reconstruction by level-sets of n-ary scattering obstacles

Amelie Litman

Reconstruction by level sets of n-ary scattering obstacles

A. Litman

Institut Fresnel UMR-CNRSTIC 6133, Université de Provence, Aix-Marseille I, Université Paul Cézanne, Aix-Marseille III, Ecole Généraliste d'Ingénieurs de Marseille, Campus de Saint-Jerôme, case 162, 13397 Marseille Cedex 20, France

E-mail: amelie.litman@fresnel.fr

Abstract. An extension of the level set representation is proposed for the reconstruction of the unknown cross-section of multiple phase material obstacles embedded in an homogeneous medium and illuminated by time-harmonic electromagnetic line sources. The a priori information assumed therein is that the scatterers are homogeneous by parts and of known characteristics. Two types of approaches are discussed with their pros and cons. In the first approach, a single level set enables to represent the different material phases. In the second approach, the material properties are coded on a binary basis and several level sets are combined, one for each bit of binary coding. Theoretical and numerical details are provided for both approaches, using synthetic and experimental measurements obtained in the anechoic chamber of Institut Fresnel.

Submitted to: *Inverse Problems for the Special Section — Testing inversion algorithms against experimental data: Inhomogeneous targets —*

1. Introduction

In inverse scattering problems, the goal is to retreive constitutive parameters of unknown scatterers from their electromagnetic signature. As this problem is highly nonlinear and ill-posed, all *a priori* information is of importance to reduce illposedness and therefore the range of plausible solutions.

We restrict ourself to a two-dimensional transmission problem where the unknown scatterers are embedded in an homogeneous background such as air. Measurements of the scattered fields at several sensors locations around the obstacle and for several locations and/or frequencies of time-harmonic E-polarized sources placed nearby are available. In particular, an experimental database has been obtained in the anechoic chamber of Institut Fresnel for several obstacles.

Additional *a priori* information is introduced as we assume that the dielectric properties of the obstacles are known and that they are constant by parts. Therefore, this inverse scattering problem is reduced to a shape optimization problem where the contour of the different scatterers is looked for. No further assumption on the connexity or the size of the objects is introduced. This configuration is an extension of the so-called *binary* obstacle case to *n-ary* obstacles, where the obstacles are made of different types of known material phases.

A significant work now exists on the retreival of binary obstacles. Some of them include this binarity by discretizing the test domain into black and white pixels [Souriau *et al* 1996]. Others are interested by the contour of the obstacle and its representative coefficients [Rozier *et al* 1997] [Bonnard *et al* 1998] and provide iterative schemes which perturbate the contour. Finally, the level-set representation has proved to be one of the most suitable representation for binary objects when no additionnal topological information is available, such as connexity for example. This level-set approach is been now used widely in various domains of inverse problem [Santosa 1996] [Litman *et al* 1998] [Dorn *et al* 2000], [Ramananjaona *et al* 2001], [Burger 2004] or shape optimization [Allaire *et al* 2004]. This level-set representation requires the computation of the shape derivative of the cost functional which links the difference between the measured and simulated scattered field. Shape derivative and topological derivative can also be mixed in order to accelerate the apparition of inclusions in the iterative process [Burger *et al* 2004].

The idea of the present paper is to extend the notion of level-set from *binary* obstacles to *n-ary* ones in order to benefit from the advantages of the level-set representation. These advantages consist for example in keeping a fixed mesh during the entire iterative process, in handling in a natural way merging and splitting of the obstacles. Several ways of representing *n-ary* obstacles by means of level-sets have already been done, for example in contour recognition for image analysis [Zhao *et al* 1996] [Samson *et al* 2000] [Osher and Paragios 2003]. But to our knowledge, these schemes have not been extended to inverse scattering configurations.

Two approaches are analysed in the present paper. The first idea is to use a single

level-set for representing all the obstacles. The computational changes introduced by the *n-ary* aspect are then minimal compared to a binary case. The second idea is to use several level-sets. One could attach a level-set to each material phase as done in [Zhao *et al* 1996]. Overlapping areas become then an issue as they are not physically possible. Instead of introducing a penalty term to prevent those overlapping areas, as done in [Samson *et al* 2000] [Osher and Paragios 2003], we prefer to follow the ideas of [Vese and Chan 2002]. The material phases are coded on a binary basis and a level-set is attached to each coding bit. The computational changes are more complex in that case but the results are improved as will be shown in the following numerical examples.

The paper is organized as follows. In section 2, the formulation of the problem is introduced. In section 3, we discuss different ways of representing an obstacle by means of level-sets, taking into account that the obstacle is homogeneous by part. These representations can rely on a single level-set or on several ones which are combined in a suitable way in order to fully represent the obstacle. In section 4, the minimization scheme based on a single level-set representation is presented in detail. In section 5, a second scheme based on a 'color' level-set evolution is proposed and analyzed. Numerical results based on a synthetic configuration are presented in section 6. Reconstructions from the new database measurements of Institut Fresnel are shown in section 7. In section 8 concludings remarks are made. In the appendices, complementary elements are introduced, in particular the adjoint field computation for the single level-set representation and the 'color' level-set one.

2. Transmission problem

The model is the following : a set of z-oriented cylindrical obstacles, of cross-section Ω_i, $i = 1, \ldots, n$, is embedded in an homogeneous space denoted by $\Omega_0 = \mathbb{R}^2 \setminus \overline{\bigcup_{i=1}^n \Omega_i}$ (figure 1). Each obstacle is assumed to be linear, isotropic, non-magnetic and penetrable and to have a sufficiently smooth boundary Γ_i. Each obstacle is characterized by a unique material property $(\varepsilon_i, \sigma_i, \mu_0)$ and is homogeneous. The set Θ of all those obstacles defined below is therefore homogeneous by part :

$$\Theta = \bigcup_{i=1}^{n} \Omega_i \quad \text{and} \quad \Omega_i \bigcap_{i \neq j} \Omega_j = \emptyset \tag{1}$$

Each exterior normal to the boundary Γ_i is denoted by $\vec{n}_i$. The wave numbers $k_i(\omega)$ ($\mathrm{Im}(k_i(\omega)) \geq 0$) of the different materials are assumed to be known for each frequency ω and to be independent of the position (the time dependance $\exp(-j\omega t)$ is chosen and dropped out from now on). An incident wave u^i of same cylindrical dependance (line source) illuminates the obstacle. We restrict ourselves to a Transverse Magnetic (TM) or E-polarization configuration. The total field u satisfies the following set of equations:

$$\Delta u + k_i^2 u = 0 \qquad \text{in } \Omega_i, \quad \forall i = 0, \ldots, n \tag{2a}$$

$$u^- = u^+ \qquad \text{on } \Gamma_i, \quad \forall i = 1, \ldots, n \tag{2b}$$

$$\frac{\partial u}{\partial \vec{n}_i}^+ = \frac{\partial u}{\partial \vec{n}_i}^- \qquad \text{on } \Gamma_i, \quad \forall i = 1, \ldots, n \tag{2c}$$

where $u^+(u^-)$ denotes the limit of u from the exterior (interior) of Ω_i. The scattered field $u^s = u - u^i$ satisfies the Sommerfeld radiation condition

$$\lim_{r\to\infty} \sqrt{r}(\frac{\partial u^s}{\partial r} - jk_0 u^s) = 0 \tag{3}$$

where $r = |x|$ and $j^2 = -1$. It has been shown that this transmission problem has a unique solution $u \in H^1_{loc}(\mathbb{R}^2)$ for a given set Θ.

The inverse problem consists in finding the shapes Ω_i, $i = 1, \ldots, n$, corresponding to each material phase which minimize the error on the data fit. If we denote by $L^2(M)$ the set of the measured scattered fields, where M is the probing line, the cost functional to minimize is of the following form:

$$J(\Theta) = \tfrac{1}{2} \parallel u^s(\Theta) - g \parallel^2_{L^2(M)} \tag{4}$$

where g corresponds to the data and Θ is our collection of shapes of known properties. The inverse problem can then be written as:

$$\text{Find } \Theta^* \text{ such that } J(\Theta^*) = \min_{\Theta} \tfrac{1}{2} \parallel u^s(\Theta) - g \parallel^2_{L^2(M)} \tag{5}$$

3. Shape representation

As stated above, the problem to tackle is reduced to a shape optimization problem. One of the main issue now is to correctly represent the shapes.

In the case of binary obstacles, one of the most suitable representation is made via the use of a level-set function [Santosa 1996]. Indeed, when using such representation, no apriori information is needed on the number of obstacles as well as the position of their centers. Furthermore topological changes such as merging or splitting are easily handled.

In the case of n-ary obstacles, the representation is less obvious. In the following, we will focus on two types of representations, both of them being based on the level-sets functions in order to keep the advantages of such implicit description.

3.1. Unique level set representation

For a single homogeneous obstacle Ω, the associated level set function $\phi \in C^1(B_R)$ is defined by (figure 2):

$$\Gamma = \{x \in B_R \mid \phi(x) = 0\} \tag{6}$$

$$\Omega = \{x \in B_R \mid \phi(x) < 0\} \tag{7}$$

With this representation, the definition of the contour is implicit and made in a geometrical fashion.

Let us therefore assume that we have several obstacles Ω_i of known characteristics, all of them being homogeneous. The idea is to simply extend the previous level set function to the n-ary case with ϕ defined by (figure 3):

$$\Gamma_i = \{x \in B_R \mid \phi(x) = c_i\} \tag{8}$$

$$\Omega_i = \{x \in B_R \mid c_{i+1} < \phi(x) < c_i\} \tag{9}$$

where the values c_i are predefined level values. Therefore, each truncation plane at the prescribed height c_i will correspond to a contour Γ_i. This representation is very simple and again implicit for each obstacle. The whole structural body Θ will then be partitionned by

$$\Theta = \bigcup_{i=1}^{n} \{x \in B_R \mid c_{i+1} < \phi(x) < c_i\} \tag{10}$$

and such partition will keep the properties that $\Omega_i \bigcap \Omega_j = \emptyset, i \neq j$.

To simplify the notation, let us introduce the one-dimensional Heaviside function H such that

$$H(x,c) = \begin{cases} 1 & \text{if } x < c \\ 0 & \text{if } x > c \end{cases} \tag{11}$$

The characteristic function of an obstacle Ω_i is then described by

$$\chi_{\Omega_i}(x) = H(\phi(x), c_{i+1}) - H(\phi(x), c_i) \tag{12}$$

where the limit levels are set to $c_0 = +\infty$ and $c_{n+1} = -\infty$.

As described in section 4, the minimization process for a single phase obstacle [Litman *et al* 1998] can easily be extended to several phases with this description. Unfortunately this approach suffers from some topological constraints that will be highlighted by the numerical results. Therefore it might be interesting to look for another description.

3.2. Vector level set representations

3.2.1. Vector level set An other idea is to provide a level set description for each material phase [Zhao *et al* 1996], i.e.,

$$\Gamma_i = \{x \in B_R \mid \phi_i(x) = 0\} \tag{13}$$

$$\Omega_i = \{x \in B_R \mid \phi_i(x) < 0\} \tag{14}$$

where the level set functions ϕ_i are all defined on $C^1(B_R)$.

This will necessitate in the minimization process to evolve each level set simultaneously and the extension from a single to a multi-phase object is not that obvious. Moreover, it can happened that the level-sets overlap during the iterative process defining therefore a region of multiple values which is not physically possible. This means that the property of (1) is not preserved by this level set representation. Usually, an additionnal constraint is introduced in the cost function with a Lagrange multiplier in order to minimize the overlap area [Zhao *et al* 1996] [Samson *et al* 2000] [Osher and Paragios 2003] but this constraint is difficult to maintain accurately. Moreover, the complexity of the algorithms increases drastically with the number of material phases.

3.2.2. 'Color' level set A different approach has been proposed in [Vese and Chan 2002] [Wang and Wang 2004]. Here, the use of multiple level sets is still being done. The main difference is the way the association is done from the material phases Ω_i to the level sets. In order to reduce the need of a mixing phase procedure, they have introduced m level sets functions to represent a structure of $(n+1) = 2^m$ different material phases, in a principle similar to combining colors from primary colors.

Suppose that we have n different types of material phases and each phase index is denoted by i. The idea is to code in a binary fashion those indexes. For n phases, there will be $m = log_2(n+1)$ coding bits and therefore m associated level sets. The level set ϕ_b associated to the bit b is such that :

$$\gamma_b = \{x \in B_R \mid \phi_b(x) = 0\} \tag{15}$$

$$\omega_b = \{x \in B_R \mid \phi_b(x) < 0\} \tag{16}$$

The domain ω_b will then define the places where the b bit of the phases indexes i is nonzero.

To simplify the notation, let us use again the Heaviside function notation. Let B_i^j a function which provides the j bit of index i. Let us introduce the function $\tilde{H}$:

$$\tilde{H}^b(y) = \begin{cases} H(y,0) & \text{if } b = 1 \\ 1 - H(y,0) & \text{if } b = 0 \end{cases} \tag{17}$$

With these notations, an obstacle Ω_i has a characteristic function defined by

$$\chi_{\Omega_i}(x) = \prod_{b=1}^{m} \tilde{H}^{B_i^b}(\phi_b(x)) \tag{18}$$

Let us illustrate this on an example with 3 different material phases apart from air, which means four different wavenumbers $\{k_0, k_1, k_2, k_3\}$. Only $m = 2$ coding bits and associated level set functions are required (figure 4) and the characteristics functions are described by:

$$\chi_{\Omega_0} = \tilde{H}^{B_{00}^1}(\phi_1)\tilde{H}^{B_{00}^2}(\phi_2) = (1 - H(\phi_1, 0))\ (1 - H(\phi_2, 0)) \tag{19}$$

$$\chi_{\Omega_1} = \tilde{H}^{B_{01}^1}(\phi_1)\tilde{H}^{B_{01}^2}(\phi_2) = H(\phi_1, 0)\ (1 - H(\phi_2, 0)) \tag{20}$$

$$\chi_{\Omega_2} = \tilde{H}^{B_{10}^1}(\phi_1)\tilde{H}^{B_{10}^2}(\phi_2) = (1 - H(\phi_1, 0))\ H(\phi_2, 0) \tag{21}$$

$$\chi_{\Omega_3} = \tilde{H}^{B_{11}^1}(\phi_1)\tilde{H}^{B_{11}^2}(\phi_2) = H(\phi_1, 0)\ H(\phi_2, 0) \tag{22}$$

This representation enables to reduce drastically the number of level-sets that will evolve during the minimization process. Furthermore, the mixing parts are avoided with such representation and no extra constraint terms in the cost function is needed. Section 5 will provide the insights of the velocity computations for each level set and some numerical examples.

4. Evolution of a unique level-set

The inverse problem of finding the set Θ^* of material phases Ω_i which satisfy (4) is solved by using an iterative scheme. A family of shapes Θ_t is constructed by perturbating an

initial shape Θ_0, for $0 \leq t \leq T$, where t is a fictitious parameter which described the iterative process. The deformation are done in order to reduce the cost function at each step.

In the case of a representation by a unique level-set, this iterative scheme is reduced to the deformation of this single level set $\phi(t,x)$.

4.1. The Hamilton-Jacobi equation

The fisrt question is to describe the deformation process for this specific level-set. If we differentiate one level contour c_i which corresponds to Γ_i, according to t, we get [Santosa 1996] :

$$\frac{\partial}{\partial t}\phi(t,x) + \vec{V}(t,x)\cdot\vec{n}\,|\nabla\phi(t,x)| = 0 \tag{23}$$

as $\partial x/\partial t = \vec{V}(t,x)$ and $\vec{n} = \nabla\phi/|\nabla\phi|$. Indeed, the level contour value c_i does not evolve with time. Therefore, for each level c_i, the evolution of the level set will be governed by the same equation. This equation is a Hamilton-Jacobi type equation, where the velocity $\vec{V}$ plays an important role [Osher and Sethian 1988] [Sethian 1999].

By using a unique level-set representation of the obstacles, the evolution of the level-set does not change from the case of a single material phase.

4.2. Fréchet derivative

The next question is to compute the Fréchet derivative of the cost functional for a given deformation of the obstacle Θ_t. It can be shown, (see Appendix A), that the Eulerian derivative of the cost functional (4) for a given velocity field $\vec{V}(t,x)$ along the normal direction can be expressed by

$$dJ(\Theta_t,\vec{V}) = -\,\mathrm{Re}\sum_{i=0}^{n} k_i^2 \int_{B_R} \left[\delta(\phi,c_{i+1}) - \delta(\phi,c_i)\right] u(x)p(x)V(t,x) \mid \nabla\phi(t,x) \mid dx \tag{24}$$

where $\delta(x,c_i)$ is a Dirac delta function concentrated on the interface Γ_i and the adjoint state p is defined by

$$\Delta p + k_i^2 p = -\overline{(u^s - g)}\,\delta_M \qquad \text{in } \Omega_i, \quad \forall i = 0,\ldots,n \tag{25a}$$

$$p^- = p^+ \qquad \text{on } \Gamma_i, \quad \forall i = 1,\ldots,n \tag{25b}$$

$$\frac{\partial p}{\partial \vec{n}}^+ = \frac{\partial p}{\partial \vec{n}}^- \qquad \text{on } \Gamma_i, \quad \forall i = 1,\ldots,n \tag{25c}$$

where δ_M denotes the Kronecker symbol on the probing line M. The adjoint problem is equivalent to the direct problem when the emitters and the receivers positions are exchanged. This comes from the reciprocity principle satisfied by the electromagnetic fields in this configuration. Both direct and adjoint problem will be solved numerically by a method of moments based on a domain integral representation of the fields.

4.3. Velocity choice

The velocity controls the evolution of the scheme and an appropriate choice is thus essential in order to provide a decrease of the cost function. Since both the Fréchet derivative (24) and the Hamilton-Jacobi equation (23) only require the normal component of the velocity, we restrict ourselves to velocities which are in the normal direction :

$$\vec{V}(t,x) = V(t,x)\vec{n}(t,x) \tag{26}$$

As done in [Litman *et al* 1998], an empirical choice of the velocity amplitude is provided by :

$$V(t,x) = \mathrm{Re} \sum_{i=0}^{n} k_i^2 \left[\delta(\phi, c_{i+1}) - \delta(\phi, c_i)\right] u(x)p(x) \quad \forall x \in B_R \tag{27}$$

4.4. Initialisation of the level set

Once the evolution of the level set is described, the next step is a correct definition of a starting point. Usually, when considering a single material phase obstacle, the level set is initialized as the signed distance function once an initial obstacle Ω is given.

$$\phi(0,x) = \begin{cases} -\mathrm{dist}(x, \partial\Omega) & \text{if } x \in \Omega \\ +\mathrm{dist}(x, \partial\Omega) & \text{if } x \notin \Omega \end{cases} \tag{28}$$

In the case of n-ary obstacles, this type of initialisation is no longer possible as there is no way to construct a unique level set which is a distance function for all Ω_i. On the other hand, the level-set representation does not require that only a signed distance function must be used, especially as the Hamilton-Jacobi equation does not preserve this property [Gomez and Faugeras 2000].

Three initialization procedures have been investigated:

- Backpropagation scheme [Kleinman and van den Berg 1992]. By applying such scheme on the data, one can get an estimation of the current density in the investigation area. The backpropagation image is then taken directly as the level set function.
- Topological asymptotic expansion [Guillaume and SidIdris 2002] [Burger *et al* 2004]. The topological asymptotic expansion corresponds to a first step of a level-set procedure by using as an initial guess no object at all. In that case, the velocity computed by means of (27) provides the same type of result and gives a good indication of the topologies. This velocity is then taken directly as the level set function.
- N-ary image. An n-ary image is provided by the end-user. As mentionned above, there is no way to compute a distance function on that image. Nevertheless, a blurring process based on a convolution filter with a gaussian kernel can be applied to provide a level set function which will have the same topology as the initial image. Unfortunately, by doing this type of blurring, the exact positions of the

boundaries are lossed. This might be troublesome when performing frequency hopping reconstructions.

Once the initial level set is obtained, the cut-off levels c_i are simply computed by performing an equirepartition in height of the level set :

$$c_i = \max(\phi) - (\max(\phi) - \min(\phi))\frac{i}{n} \tag{29}$$

The first and last levels are set respectively to $+\infty$ and $-\infty$ in order to cover the entire range of values.

5. 'Color' level set

By using a 'color' level set representation for n multiple phase materials, we need to change the iterative scheme. Indeed, instead of deforming a unique level-set along time, the deformation must be done on a full set of level-sets $\phi_b(t,x)$, one for each coding bit as described previously. This implies that the velocity for each level set must be defined carefully.

5.1. The Hamilton-Jacobi equation

For each level set ϕ_b, the deformation process is still governed by an Hamilton-Jacobi type equation of the following form :

$$\frac{\partial}{\partial t}\phi_b(t,x) + \vec{V}_b(t,x)\cdot\vec{n}_b\,|\nabla\phi_b(t,x)| = 0 \;\; \forall b = 1,\ldots,m \tag{30}$$

where $\partial x/\partial t = \vec{V}_b(t,x)$ and $\vec{n}_b = \nabla\phi_b/\mid\nabla\phi_b\mid$ and $m = \log_2(n+1)$ is the number of coding bit required. Each level set evolution will then be performed seperately for each specific velocity field on the same fixed grid. The time step is chosen in order to satisfy the CFL condition for all level set functions.

5.2. Fréchet derivative

As the representation of the obstacles has changed, the Fréchet derivative of the cost function will be different. It can be shown, (see Appendix B), that the Eulerian derivative of the cost functional (4) for a given set of velocity fields $\vec{V}_b$ along the normal directions can be expressed by

$$dJ(\Theta_t, \left\{\vec{V}_b\right\}) = -\mathrm{Re}\sum_{i=0}^{n} k_i^2 \sum_{b=1}^{m}\int_{B_R}\left(\prod_{j=1,j\neq b}^{m}\tilde{H}^{B_i^j}(\phi_j)\right)u(x)p(x)\tilde{\delta}^{B_i^b}(\phi_b)V_b\mid\nabla\phi_b\mid dx \tag{31}$$

where the adjoint state p is still defined by $(25c)$ and $\tilde{\delta}^{B_i^b}(\phi_b)$ is a Dirac delta function concentrated on the 0-level of ϕ_b with a positive or negative sign according to B_i^b.

5.3. Velocity choice

In order to provide a scheme which tends towards the best shape Θ^*, the velocities V_b must be chosen in order to minimize the cost functional at each step. An empirical choice is provided by

$$V_b(t,x) = \mathrm{Re}\sum_{i=0}^{n} k_i^2 \left(\prod_{j=1, j\neq b}^{m} \tilde{H}^{B_i^j}(\phi_j) \right) \tilde{\delta}^{B_i^b}\, u(x)p(x) \tag{32}$$

for each level set function ϕ_b associated to the bit b.

6. Numerical results from synthetic data

The two algorithms have been tested in various configurations. A detailed analysis based on synthetic scattered fields is first provided in order to test the influence of the initial guess and to show the pros and cons of each approach.

6.1. Description of the synthetic configuration

The homogenenous background in which the obstacles are located is air $(\varepsilon_0, \sigma_0 = 0, \mu_0)$. The area in which the obstacles can be found is a square test domain of length side $d = 2\lambda$ and centered at $(0,0)$. Ony one frequency is used, 10 GHz ($\lambda = 3cm$). The receivers and the sources are equally spaced on a circle of radius 3λ and centered at $(0,0)$. The number of receivers and emitters are identical, i.e., 36. The obstacles under study consist of two disks (figure 5). The first one is of radius $\lambda/4$, centered at $(\lambda/4, \lambda/4)$ made of $(\varepsilon_1 = 1.5\varepsilon_0, \sigma_1 = 0, \mu_0)$. The second one is of radius $\lambda/4$, centered at $(-\lambda/2, -\lambda/2)$ made of $(\varepsilon_1 = 2\varepsilon_0, \sigma_2 = 0, \mu_0)$. The color assocation is done such as blank correspond to air $(n = 0)$, grey to the materia $(n = 1)$ made of $(\varepsilon_1 = 1.5\varepsilon_0, \sigma_1 = 0, \mu_0)$ and black to the last materia $(n = 2)$.

6.2. Numerical considerations

The scattering phenomenon is modeled by a method of moments for the direct and inverse problems. The test domain is divided into square cells. The number of cells varies between the direct problem (43×43) and the inverse one (21×21) in order to prevent ourselves from committing an inverse crime. In both cases, the size of the cells is sufficiently small according to the Method of Moments criteria.

The Hamilton-Jacobi equation is solved on a fixed Cartesian grid using a stable and entropy satisfying scheme developped by [Osher and Sethian 1988] [Sethian 1999]. The time step is automatically selected in order to satisfy the CFL condition and will be taken as $\Delta t = 0.5 * \Delta t_{CFL}$ in order to assure a slow but smooth convergence.

The Heaviside function and its derivate are approximated by the following functions as in [Vese and Chan 2002]:

$$H(\phi, c) = 1 - \frac{1}{2}(1 + \frac{2}{\pi}\arctan(\frac{\phi - c}{0.1})) \qquad \delta(\phi, c) = -\frac{1}{\pi}\frac{0.01}{0.01 + (\phi - c)^2} \tag{33}$$

The iteration process is stopped if the cost function is low enough (< 0.3) or if the number of iterations has reached 100. The cost function correspond to the difference between the measured and simulated scattered fields normalised by the measured scattered fields.

6.3. Single level-set evolution

6.3.1. Initialisation Three different types of initial level set functions has been investigated: (i) an initial cercle made of ($\varepsilon = 1.5\varepsilon_0, \sigma = 0, \mu_0$), centered and of radius $2\lambda/3$ blurred by a convolution with a Gaussian filter (figure 6 (a)) (ii) the retropagation result (figure 6 (b)), (iii) the velocity field obtained with a null initial guess (figure 6 (c)). The last two ones provides a good estimation of the positions of the scatterers as well as their contrasts.

6.3.2. Cost function Due to the different initialisation procedures, the cost function evolution is presented in figure 7 (a). The oscillations in the cost function at the end of the iteration is due to to the solution which evolve in a non-smooth way when looking at small scale changes compared to the pixel size. It can be seen that the initialisation process has some effect on the convergence of the algorithm and the value of the cost function at the end is more important when using a single centered circle as initial guess.

6.3.3. Image and level-set evolution When initializing by a centered circle, the algorithm does not converge towards the 'exact' solution (figure 8 (a)). The positions of the objects are correctly found but the shape and the value of associated permittivity are different. Indeed, by having more material properties available, the number of degree of freedom has increased and the solution obtained is an equivalent one where the scatterer of largest permittivity is replaced by a scatterer of larger area with reduced permittivity. Figure 9 shows the evolution of the associated level-set function, when the initialisation is done with a circle, and one can see the decrease of the amplitude of the level-set and its spreading.

If more apriori information is introduced in the initial guess, as it is done with the other two initialisation processes, the resulting image is very close from the 'exact' one (figure 8 (b) and (c)). Nevertheless, fast transitions from one material to an other are not handled by a single level-set representation. This is a severe drawback of such representation which can slightly be reduced with a more refined mesh but will still be present.

6.4. 'Color' level-set evolution

6.4.1. Initialisation Due to the presence of 3 different material phases, two level-set functions are necessary to represent the coding bits. Two types of initialisation process has been investigated: (i) an initial cercle made of ($\varepsilon = 2\varepsilon_0, \sigma = 0, \mu_0$), centered and of radius $\lambda/2$ (figure 10 (a)), which provides two level-sets which are identical, (ii) the

retropropagation result (figure 10 (b)) truncated into two layers to initialize the two level-set functions.

6.4.2. Cost function Figure 7(b) shows the evolution of the cost function for different initial guesses. Here, the initialisation with a circle provides faster convergence, but this can change from one configuration to another one.

6.4.3. Image and level-set evolution Figure 11 show the resulting image for the different initial guesses. The reconstruction is very satisfactory with this type of approach and one can distinctly recognized the two scatterers made of different materia. The evolution of the associated level-set functions is presented in figure 12. One can see easily the bit association that results in the n-ary images of figure 11.

7. Numerical results from experimental data

The anechoic chamber of Institut Fresnel was used to mesure the scattered fields from various objects illuminated at different angles and frequencies. A detailed description of the setup is provided in [Geffrin *et al*]. In the present article, only the Transverse Magnetic measurement is analyzed but the same algorithm can be extended to the Transverse Electric case [Ramananjaona *et al* 2001] with a suitable definition of the adjoint fields. All incident and receivers measurements are used. The scattered fields are normalized as explained in [Tijhuis *et al* 2001] by defining a complex coefficient which assumes that the point opposite to the antenna is measuring an incident field which is equivalent to the field radiated by a line source.

7.1. Numerical considerations

As previously, a method of moments was used for modelling the electromagnetic phenomenon. The number of cells was taken as (31×31) and the domain test was a centered square box of (0.2×0.2) m. The Hamilton-Jacobi equation was solved as previously with the same Δt condition and the same Heaviside function as in (33). The iteration process was stopped when the cost function was low enough or after 30 iterations. All reconstructions are presented with the same initial guess, corresponding to a circle, centered, of radius 0.05 m. The color association is done such as $(n = 0)$ correspond to air, $(n = 1)$ correspond to the dielectric of permittivity $\varepsilon_r = 1.45$ and $(n = 2)$ correspond either to the dielectric of permittivity $\varepsilon = 3$ or to the metal part. When the obstacle is metallic, its permittivity is taken as $\varepsilon_r = 1$ and its conductivity is taken as $\sigma = 1$ S/m to be sure that the cell size is larger than the skin depth.

7.2. Cost functions

For all configurations, the cost functions are presented with the same initial guess in figure 13. In the dielectric cases, the convergence is again very rapid and oscillations

appear when the size of the image changes are of the order of the cell size. When there are metallic parts, the convergence process is slower and in fact does not converge when using a single level-set representation.

7.3. Reconstructions at 2 GHz

Reconstructions obtained after 30 iterations for the different dielectric configurations are presented in figure 14 for the FoamDielIntTM case, in figure 15 for the FoamDielExtTM case, and in figure 16 for the FoamTwinDielTM case. All reconstructions are very satisfactory even when using a single frequency. This highlights the importance of a priori information introduced into the inversion algorithm.

Reconstructions obtained after 100 iterations for the FoamMetExtTM case are presented in figure 17. The single level-set representation did not converge as the 'color' level-set representation did. Indeed, when there are metallic parts, the convergence is more difficult to achieve as the velocity computation requires the value of the total field inside the object. If the object is metallic, the field will be close to zero and the associated velocity will be null inside. This means that the inner points will not be removed even if needed and this will prevent proper convergence.

7.4. Reconstructions at higher frequency

Unfortunately, due to the way the initialisation process is done with the single level-set representation, it is not possible to perform a frequency-hopping approach as in [Tijhuis *et al* 2001]. Indeed, the initial guess does not fully preserve the topology obtained at previous frequencies as some blurring procedure is applied to the binary image in order to create an artificial level-set function.

Therefore only frequency-hoping results are presented for the 'color' level-set approach in figure 18 for the FoamTwinDielTM case. In order to provide a discretisation grid which respects for all frequencies the method of moments ratio of $\lambda/7$, the number of cells has been increased to 41×41. Three frequencies have been used at 2, 4 and 6 GHz. The last iteration, i.e., iteration 100, is used as an initial guess for the next frequency. In fact, as the reconstructions are already of a very good quality at 2 GHz, the higher frequencies do not provide much further information.

8. Conclusion

We have presented here two types of approaches for representing *n-ary* obstacles by means of level-set. The first approach is based on a single level-set representation and is simplier to implement than the second one which uses several level-sets, one for each coding bit necessary to code the material phases on a binary basis.

As we have seen in the numerical examples, the two approaches are reacting differently to initial guess selection. The first one is more sensible than the 'color' level-set representation. Furthermore, the first approach is not really appropriate when

there are sharp transitions, from material ($n = 0$) to material ($n = 2$) for example. This case is better reconstructed with the 'color' level-set. Finally, the single level-set approach fails to converge in some situation, for example when there is a metallic part inside the scatterers, as the 'color' level-set does not. In any case, the 'color' level-set provides very satisfactory results even when using a single low frequency, as can be seen on the reconstructions obtained from the experimental fields measured in the anechoic chamber of Institut Fresnel. This prove the importance of a proper introduction of *a priori* information into the inversion process.

Acknowledgments

The author would like to thank the microwave experimental team of Institut Fresnel for providing the data, as well as K. Belkebir and M. Saillard for organizing this second special section on 'Testing inversion algorithms against experimental data'. The author gratefully acknowledge helpful discussions with H. Tortel.

Appendix A. Fréchet derivative for a single level-set

Appendix A.1. Weak formulation of the transmission problem

The objective functional to derivative is the following :

$$J(\Theta) = \tfrac{1}{2} \parallel u^s(\Theta) - g \parallel^2_{L^2(M)} \tag{A.1}$$

under the constraints that the total field u satistifies $(2c)$ or in a weak sense [Hettlich 1995]:

$$\mathcal{S}(u,v) = \int_{B_R} (\nabla u \nabla \bar{v} - \kappa^2 u \bar{v} dx) - < Lu, v >= (f,v)_{H^1(B_R)} \tag{A.2}$$

for all $v \in H^1(B_R)$, where B_R is a ball of radius $R > 0$, where $\mathcal{S}$ is a sesquilinear form: $H^1(B_R) \times H^1(B_R) \rightarrow \mathbb{C}$, where L is the Dirichlet-to-Neumann map: $H^{1/2}(\partial B_R) \rightarrow H^{-1/2}(\partial B_R)$ and $f \in H^1(B_R)$ is a linear functional linked to the incident field. The contrast κ^2 is defined by:

$$\kappa^2(x) = \sum_{i=0}^{n} k_i^2 \chi_{\Omega_i}(x) \tag{A.3}$$

where k_i^2 corresponds to the wave number of the obstacle Ω_i.

Appendix A.2. Lagrangian formulation

Let us introduce the Lagrangian function $\mathcal{L}$ defined by :

$$\mathcal{L}(u,v,t) = J(u) + \mathrm{Re}\left(\mathcal{S}(u,v,\Theta_t) - (f,v)_{H^1(B_R)}\right) \tag{A.4}$$

where Θ_t is the collection of obstacles shapes at time t. Finding the minimum of the cost functional is then equivalent to finding the saddle-point of this functional [Ramananjaona *et al* 2001]. The partial derivative $\partial\mathcal{L}(u,v,\Theta)/\partial v$ provides the weak formulation (A.2) for the total field u. The partial derivative $\partial\mathcal{L}(u,v,t)/\partial u$ provides the weak formulation for the adjoint field $p = \bar{v}$:

$$\mathcal{S}(w,v) = -\int_M \overline{(u^s - g)}(y) w(y) dy \tag{A.5}$$

$\forall w \in H^1(B_R)$, where the receivers act as sources with a prescribed amplitude.

Appendix A.3. Cost functional derivation

The next step is to derive the objective functional according to the time deformation. We have :

$$\frac{dJ}{dt} = \frac{\partial \mathcal{L}}{\partial t}(u,v,t) \tag{A.6}$$

where u is the total field defined by (A.2) and $p = \bar{v}$ is the adjoint field defined by (A.5). As the only term which moves according to time is the wave number κ^2, we get:

$$\frac{\partial \mathcal{L}}{\partial t}(u,v,t) = -\mathrm{Re} \int_{B_R} \frac{\partial \kappa^2(t,x)}{\partial t} u(x) \bar{v}(x) dx \tag{A.7}$$

In fact, the shape information is contained into the level-set representation and with a single level-set representation, this wave number is defined by:

$$\kappa^2(t,x) = \sum_{i=0}^{n} k_i^2 \left[H(\phi(t,x), c_{i+1}) - H(\phi(t,x), c_i] \right) \tag{A.8}$$

where H is the one-dimensional Heavisde function and $\phi(t,x)$ the level set at time t. For a given velocity field $V(t,x)$ which represents the perturbation vector field in the normal direction, the derivative is given by:

$$\frac{\partial \kappa^2(t,x)}{\partial t} = \sum_{i=0}^{n} k_i^2 \left[\frac{\partial H}{\partial \phi}(\phi, c_{i+1}) - \frac{\partial H}{\partial \phi}(\phi, c_i) \right] \frac{\partial \phi}{\partial t} \tag{A.9}$$

$$= \sum_{i=0}^{n} k_i^2 \left[\delta(\phi, c_{i+1}) - \delta(\phi, c_i) \right] V \mid \nabla \phi \mid \tag{A.10}$$

as ϕ follows the Hamilton-Jacobi equation (23). The function $\delta(\phi, c_i)$ corresponds to the Dirac delta function concentrated on the interface c_i [Osher and Paragios 2003]. For c_0 and c_{n+1}, this Dirac delta function has a null support and therefore does not interfere in the computations.

The derivative of the Lagrangian is then given by:

$$\frac{\partial \mathcal{L}}{\partial t}(u,p,t) = -\mathrm{Re} \sum_{i=0}^{n} k_i^2 \int_{B_R} \left[\delta(\phi, c_{i+1}) - \delta(\phi, c_i) \right] u(x) p(x) V(t,x) \mid \nabla \phi(t,x) \mid dx \tag{A.11}$$

Appendix B. Fréchet derivative for a 'color' level set

Appendix B.1. Weak formulation and Lagrangian

The cost functional to minimize, as well as the Lagrangian formulation or the adjoint state are identical as the ones described in Appendix A. As the main difference relies in the representation of the obstacles, the derivative according to time of the objective functional will be different.

Appendix B.2. Cost functional derivation

Let us again express the wave number κ^2 in terms of the level set description. Here we have $m = \log_2(n+1)$ level set functions, each for each coding bit of material phases. Following the definitions of (17) and (18), the wave number is given by:

$$\kappa^2(t,x) = \sum_{i=0}^{n} k_i^2 \left(\prod_{b=1}^{m} \tilde{H}^{B_i^b}(\phi_b) \right) \tag{B.1}$$

For a given set of velocity fields $V_b(t,x)$ for each level set function $\phi_b(t,x)$, the derivative of the wave number is :

$$\frac{\partial \kappa^2(t,x)}{\partial t} = \sum_{i=0}^{n} k_i^2 \frac{\partial}{\partial t} \left(\prod_{b=1}^{m} \tilde{H}^{B_i^b}(\phi_b) \right) \tag{B.2}$$

$$= \sum_{i=0}^{n} k_i^2 \sum_{b=1}^{m} \left(\prod_{j=1, j\neq b}^{m} \tilde{H}^{B_i^j}(\phi_j) \right) \tilde{\delta}^{B_i^b}(\phi_b) \frac{\partial \phi_b}{\partial t} \tag{B.3}$$

$$= \sum_{i=0}^{n} k_i^2 \sum_{b=1}^{m} \left(\prod_{j=1, j\neq b}^{m} \tilde{H}^{B_i^j}(\phi_j) \right) \tilde{\delta}^{B_i^b}(\phi_b) V_b \mid \nabla \phi_b \mid \tag{B.4}$$

where $\tilde{\delta}^b(\phi)$ is the Dirac delta function concentrated on the interface of the level set ϕ with a positive (resp. negative) sign if the associated bit is 1 (resp. 0).

The derivative of the objective function is then given by:

$$\frac{\partial \mathcal{L}}{\partial t}(u,p,t) = -\mathrm{Re} \sum_{i=0}^{n} k_i^2 \sum_{b=1}^{m} \int_{B_R} \left(\prod_{j=1, j\neq b}^{m} \tilde{H}^{B_i^j}(\phi_j) \right) u(x) p(x) \tilde{\delta}^{B_i^b}(\phi_b) V_b \mid \nabla \phi_b \mid dx \tag{B.5}$$

References

[Allaire *et al* 2004]Allaire G, Jouve F and Toader A. M 2004 Structural optimization using sensitivity analysis and a level-set method *J. Comp. Phys.* **194** 363–393

[Bonnard *et al* 1998]Bonnard S, Vincent P and Saillard M 1998 Cross-borehole inverse scattering using a boundary finite-element method *Inverse Problems* **14** 521–534

[Burger 2004]Burger M 2004 Levenberg-Marquardt level set methods for inverse obstacle problems *Inverse Problems* **20** 259–282

[Burger *et al* 2004]Burger M, Hackl B and Ring W 2004 Incorporating topological derivative into level set methods *J. Comput. Phys.* **194** 344–362

[Dorn *et al* 2000]Dorn O, Miller E. L and Rappaport C. M 2000 A shape reconstruction method for electromagnetic tomography using adjoint fields and level sets *Inverse Problems* **16** 1119–1156

[Geffrin *et al*]Geffrin J. M, Sabouroux P and Eyraud C Free space experimental scattering database continuation: experimental setup and measurement precision *Inverse Problems, submitted*

[Gomez and Faugeras 2000]Gomez J and Faugeras O 2000 Reconciling Distance Functions and Level Sets *J. Visual Comm. Image Representation* **11** 209–223

[Guillaume and SidIdris 2002]Guillaume P and SidIdris K 2002 The Topological Asymptotic Expansion for the Dirichlet Problem *SIAM J. Cont. Opt.* **41** 1042–1072

[Hettlich 1995]Hettlich F 1995 Fréchet derivative in inverse obstacles scattering *Inverse Problems* **11** 371–382

[Kleinman and van den Berg 1992]Kleinman R and van den Berg P 1992 A Modified Gradient Method for Two-Dimensional Problems in Tomography *J. Comput. Appl. Math.* **42** 17–35

[Litman *et al* 1998]Litman A, Lesselier D and Santosa F 1998 Reconstruction of a two-dimensional binary obstacle by controlled evolution of a level-set *Inverse Problems* **14** 685–706

[Osher and Paragios 2003]Osher S and Paragios N 2003 *Geometric Level Set Methods in Imaging, Vision and Graphics* (Telos: Springer-Verlag)

[Osher and Sethian 1988]Osher S and Sethian J. A 1988 Fronts Propagating with Curvature-Dependent Speed: Algorithms based on Hamilton-Jacobi Formulations *J. Comput. Phys* **79** 12–49

[Ramananjaona *et al* 2001]Ramananjaona C, Lambert M, Lesselier D and Zol/'esio J 2001 Shape reconstruction of buried obstacles by controlled evolution of a level set : from a min-max formulation to numerical experimentation *Inverse Problems* **17** 1087–1111

[Rozier *et al* 1997]Rozier C, Lesselier D, Angell T and Kleinmann R. E 1997 Shape retreival of an obstacle immersed in shallow water from a single frequency fields using a complete family method *Inverse Problems* **13** 487–508

[Samson *et al* 2000]Samson C, Blanc-Feraud L, Aubert G and Zerubia J 2000 A Level Set Model for Image Classification *Int. J. Comput. Vision* **40** 187–198

[Santosa 1996]Santosa F 1996 A Level-Set Approach for Inverse Problems Involving Obstacles *ESAIM: COCV* **1** 17–33

[Sethian 1999]Sethian J 1999 *Level Set Methods and Fast Marching Methods* Cambridge Monographs on Applied and Computational Mathematics (New York: Cambridge University Press)

[Souriau *et al* 1996]Souriau L, Duchene B, Lesselier D and Kleinmann R. E 1996 A modified gradient approach to inverse scattering for binary objects in stratified media *Inverse Problems* **12** 463–481

[Tijhuis *et al* 2001]Tijhuis A, Belkebir K, Litman A and de Hon B 2001 Multiple-frequency distorted-wave Born approach to 2D inverse profiling *Inverse Problems* **17** 1635–1644

[Vese and Chan 2002]Vese L and Chan T 2002 A Multiphase Level Set Framework for Image Segmentation using the Mumford and Shah Model *Int. J. Comput. Vision* **50** 271–293

[Wang and Wang 2004]Wang M and Wang X 2004 'Color' Level Sets: a Multi-Phase Method for Structural Topology Optimization with Multiple Materials *Comput. Methods Appl. Mech. Engrg.* **193** 469–496

[Zhao *et al* 1996]Zhao H, Chan T, Merriman B and Osher S 1996 A Variational Level Set Approach to Multiphase Motion *J. Comput. Phys.* **127** 179–195

Figure captions

Figure 1 : Several scattering obstacles

Figure 2 : Level-set function for a binary obstacle

Figure 3: Single level-set function for n-ary obstacles

Figure 4: Several level-set functions for n-ary obstacles

Figure 5: Synthetic configuration

Figure 6: Three initialisation processes for a single level-set representation

Figure 7: Cost function for different initial guesses

Figure 8: Resulting images with a single level-set representation for different initial guesses

Figure 9: Single level-set evolution with a circle as initial guess

Figure 10: Two initialisation processes for a 'color' level-set representation

Figure 11: Resulting images for different initial guesses with a color level-set representation

Figure 12: 'Color' level-sets evolution with a circle as initial guess

Figure 13: Cost function for the different experimental configurations

Figure 14: Resulting images for the FoamDielIntTM case

Figure 15: Resulting images for the FoamDielExtTM case

Figure 16: Resulting images for the FoamTwinDielTM case

Figure 17: Resulting images for the FoamMetExtTM case

Figure 18: Frequency-hopping images for the FoamTwinDielTM case with a 'color' level-set representation

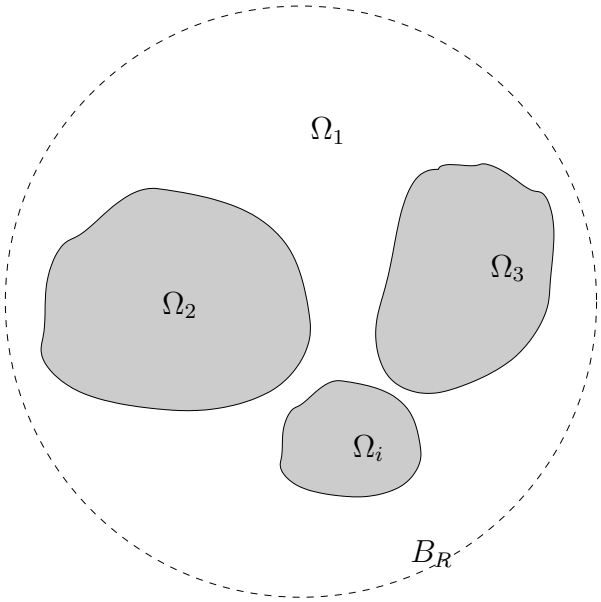

Figure 1. Several scattering obstacles

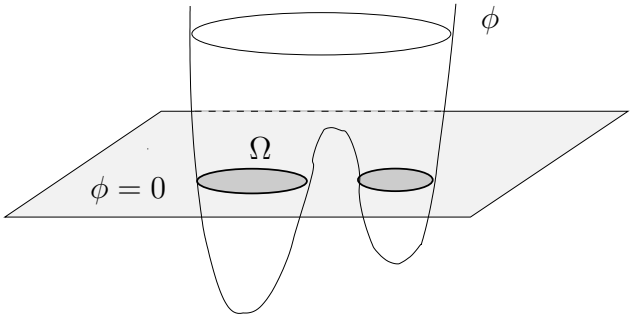

Figure 2. Level-set function for a binary obstacle

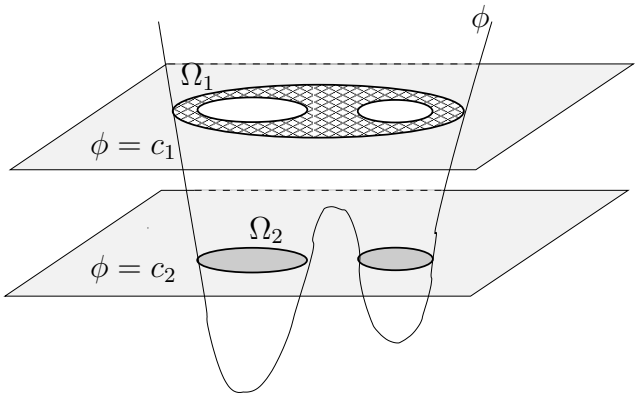

Figure 3. Single level-set function for n-ary obstacles

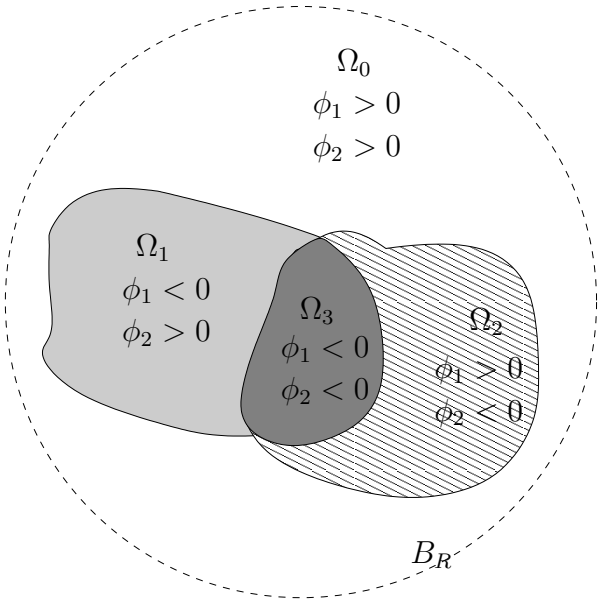

Figure 4. Multiple level-set functions for n-ary obstacles

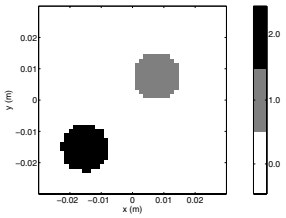

Figure 5. Synthetic obstacle configuration

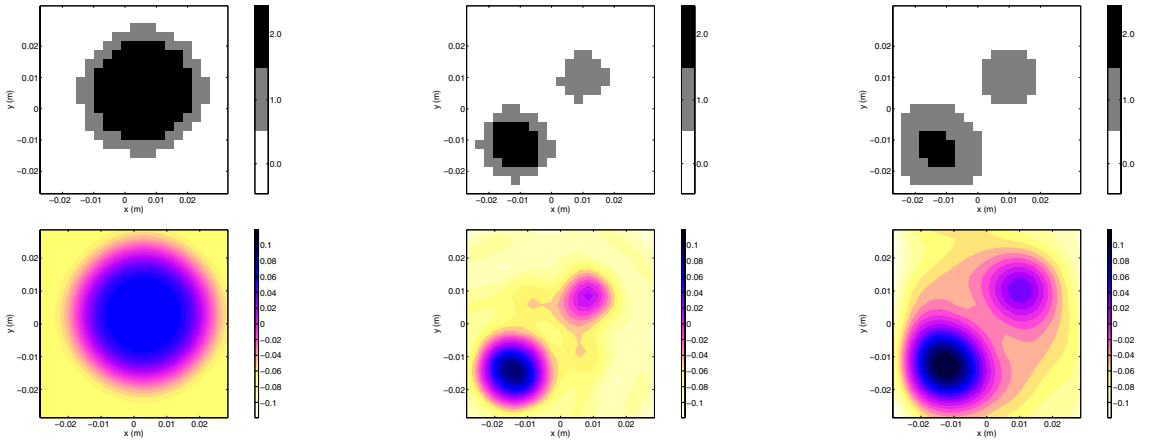

(a) Circle (b) Retropropagation (c) Velocity

Figure 6. Three initialisation processes for a single level-set representation (up) image, (down) level-set

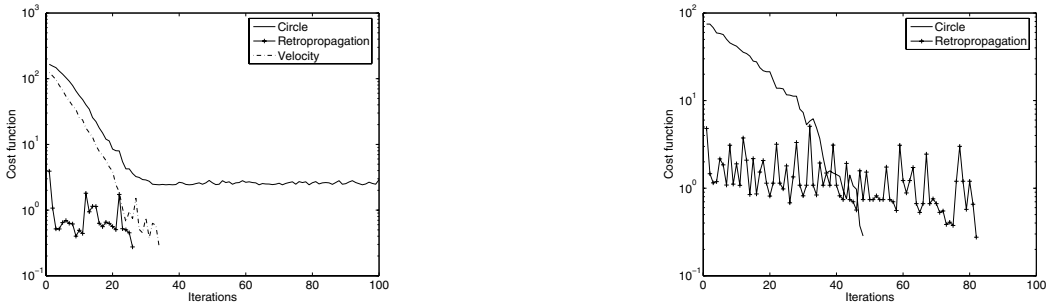

(a) Single level-set (b) Color level-set

Figure 7. Cost function for different initial guesses (——) Circle, (+) Retropropagation, (— · —) Velocity

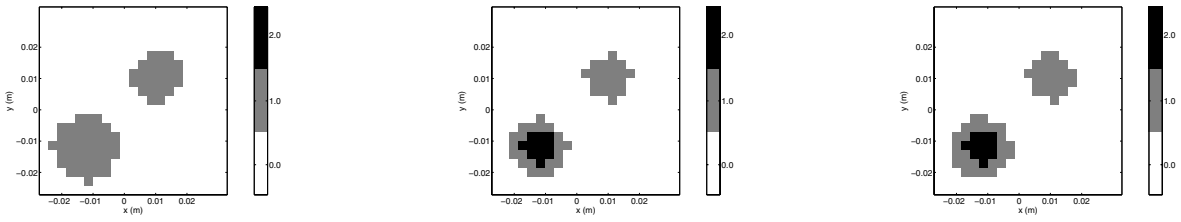

(a) Circle, it. 100 (b) Retro, it. 25 (c) Velocity, it. 34

Figure 8. Resulting images with a single level-set representation for different initial guesses

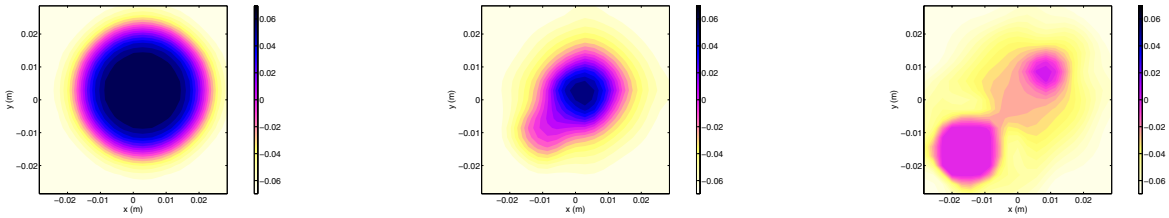

(a) Iteration 0 (b) Iteration 10 (c) Iteration 100

Figure 9. Single level-set evolution with a circle as initial guess

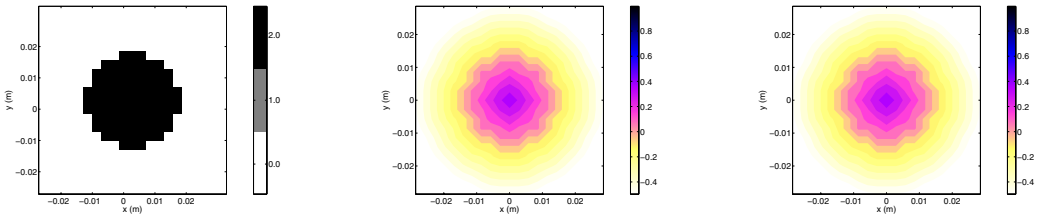

(a) Circle

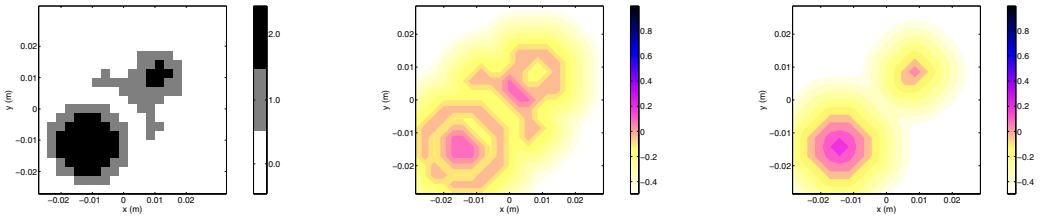

(b) Retropropagation

Figure 10. Two initialisation processes for a 'color' level-set representation (left) Image, (middle) Level-set for first bit, (right) Level-set for second bit

(a) Circle, it. 48 (b) Retro, it. 82

Figure 11. Resulting images for different initial guesses with a color level-set representation

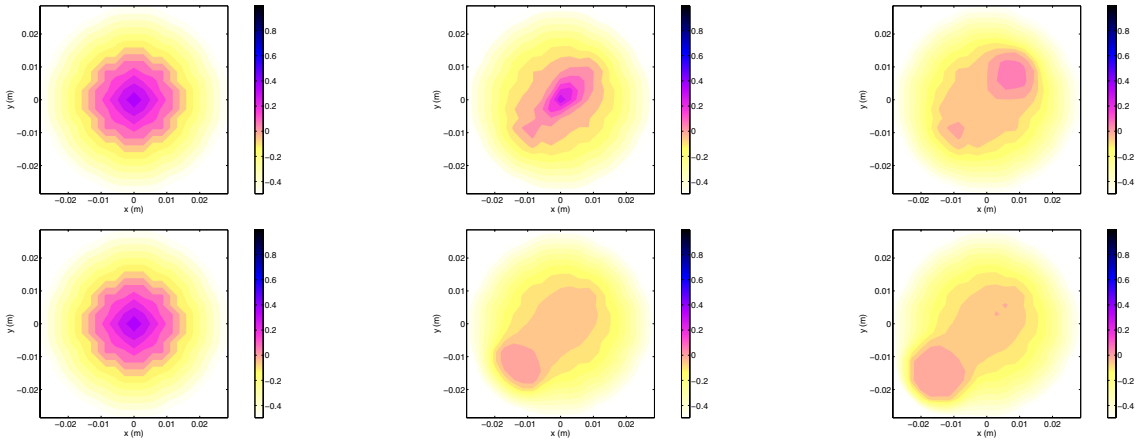

(a) Iteration 0 (b) Iteration 24 (c) Iteration 48

Figure 12. 'Color' level-sets evolution with a circle as initial guess
(up) Level-set for first coding bit, (down) Level-set for second coding bit

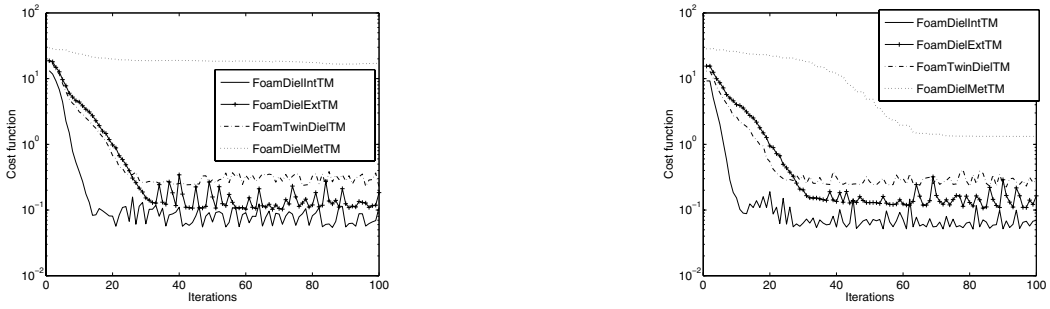

(a) Single level-set (b) Color level-set

Figure 13. Cost function for the different experimental configurations
(——) FoamDielIntTM, (+) FoamDielExtTM, (— · —) FoamTwinDielTM, (· · · · · ·) FoamMetExtTM

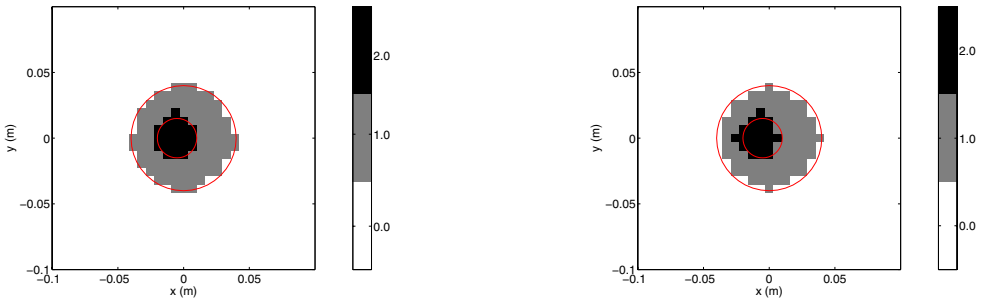

(a) Single level-set (b) Color level-set

Figure 14. Resulting images for the FoamDielIntTM case

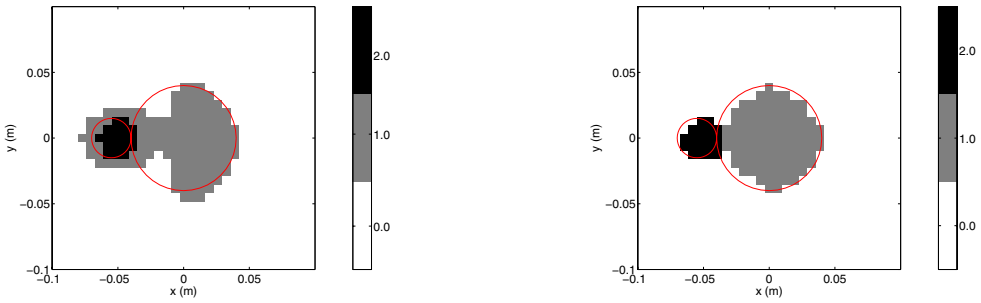

(a) Single level-set (b) Color level-set

Figure 15. Resulting images for the FoamDielIntTM case

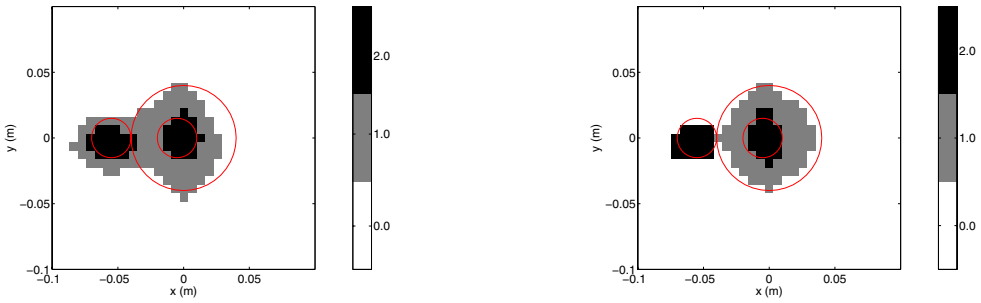

(a) Single level-set (b) Color level-set

Figure 16. Resulting images for the FoamTwinDielTM case

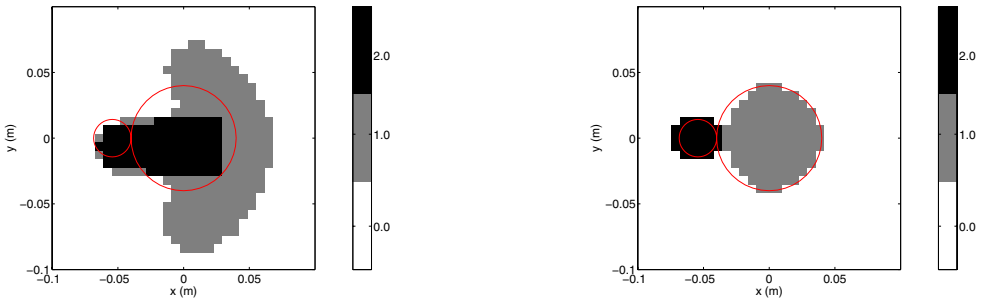

(a) Single level-set (b) Color level-set

Figure 17. Resulting images for the FoamMetExtTM case

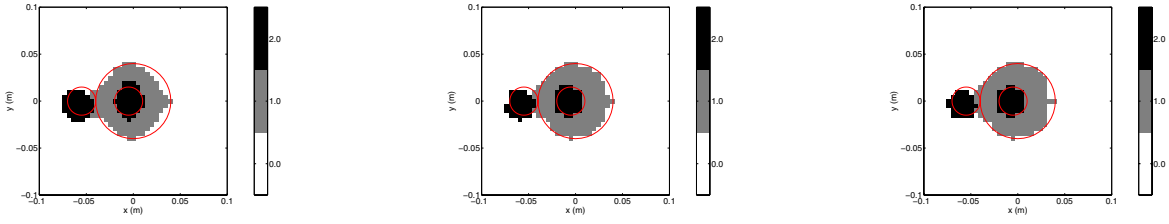

(a) 2 GHz, it. 100 (b) 4 GHz, it. 100 (c) 6 GHz, it. 100

Figure 18. Frequency hopping for the FoamTwinDielTM case